

Semiconducting ferroelectric perovskites with intermediate bands via B -site Bi^{5+} doping

Lai Jiang,¹ Ilya Grinberg,¹ Fenggong Wang,¹ Steve M. Young,¹ Peter K. Davies,² and Andrew M. Rappe^{1,2,*}¹*The Makineni Theoretical Laboratories, Department of Chemistry, University of Pennsylvania, Philadelphia, Pennsylvania 19104–6323, USA*²*Department of Materials Science and Engineering, University of Pennsylvania, Philadelphia, Pennsylvania 19104–6272, USA*

(Received 28 March 2014; revised manuscript received 28 June 2014; published 29 August 2014)

We propose B -site Bi^{5+} -doped ferroelectric perovskite materials as suitable candidates for the bulk photovoltaic effect and related solar applications. The low-lying $6s$ empty states of the electronegative Bi atom produce empty bands in the energy gap of the parent materials, effectively lowering the band gap by 1–2 eV, depending on the composition of the ferroelectric end member and the concentration of Bi^{5+} in the solid solution. The polarization decreases but survives upon doping, which enables the “shift-current” mechanism for photocurrent generation, while the decreased band gap allows absorption of much of the visible spectrum. The magnitude of shift-current response is calculated for $0.75\text{Pb}_2\text{InNbO}_6-0.25\text{Ba}_2\text{InBiO}_6$ (PIN-BIB) and $0.75\text{Pb}_2\text{ScNbO}_6-0.25\text{Ba}_2\text{ScNbO}_6$ (PSN-BSB) and is predicted to exceed the visible-light bulk photovoltaic response of all previously reported materials, including BiFeO_3 . Furthermore, the existence of their intermediate bands and multiple band gaps, combined with Fermi-level tuning by A -site co-doping, also allows for their potential application in traditional $p-n$ junction-based solar cells as broad-spectrum photoabsorbers.

DOI: [10.1103/PhysRevB.90.075153](https://doi.org/10.1103/PhysRevB.90.075153)

PACS number(s): 71.20.–b, 71.20.Nr, 71.28.+d

I. INTRODUCTION

The capture and conversion of solar energy has recently been of great interest due to its abundance, accessibility, and sustainability. However, the efficiency of the current commercially available $p-n$ junction-based solar cells is limited by the Shockley-Queisser (SQ) limit [1]. Additionally, fabrication of solar cells is complicated by the need to form an interface to enable excited carrier separation. Polar materials, on the other hand, can generate current throughout the bulk when illuminated due to the lack of inversion symmetry [2–5]. Several mechanisms have been proposed to explain the bulk excited carrier separation in ferroelectrics (FEs) and the above-band-gap photovoltages that have been observed in FE-based cells [6–11]. Among them, the shift-current mechanism, in which photoexcited coherent states possess intrinsic momentum and generate photocurrent, has been shown to corroborate experimental observations [12]. FE ABO_3 perovskite oxides such as $\text{Pb}(\text{Zr}_{1/2}\text{Ti}_{1/2})\text{O}_3$ [13] and BiFeO_3 [14–16] have been the subject of most of the solar absorber FE investigations due to their large polarizations and robustness. However, these FE oxides have band gaps (E_g) above or near the visible edge (≥ 3 eV) and therefore cannot absorb most of the solar spectrum [17–21]. This has inspired theoretical and experimental efforts to find FE oxide materials with low band gaps [22–24]. We have previously reported that introducing a combination of Ni ions and oxygen vacancies into FE perovskites gives rise to a smaller gap in the visible range by modifying the relative energy levels of the band edges [22,23]. A visible-light FE photovoltaic has been recently predicted and experimentally demonstrated [25].

In this study, we opt for a different approach: band-gap reduction is achieved by introducing low-lying empty intermediate bands (IBs) in the middle of the band gap through dopant substitutions. In addition to the benefit of a reduced band gap, the presence of a band in between the valence band

(VB) and conduction band (CB) also opens the possibility of co-doping with donors to make the intermediate band half filled. Materials with such half-filled IBs, mostly highly mismatched alloys, have been predicted to be as efficient as multijunction solar cells, while avoiding the complexity of traditional multijunction or tandem device structures. The theoretical conversion efficiency of a single IB solar cell can be up to 62%, and even higher efficiency of up to 72% is predicted for materials with two IBs [26–29].

We choose the Bi^{5+} cation as a substituent on the B site of FE perovskites to create the IB state. Previous studies have shown that $\text{Ba}_2\text{ReBiO}_6$ (rare earth $\text{Re} = \text{La}, \text{Ce}, \text{Nd}, \text{Sm}, \text{Eu}, \text{Gd}, \text{Dy}$) double perovskites have a low-lying IB comprising Bi $6s$ and O $2p$ orbitals, with an additional CB ≈ 1.5 eV higher comprising Re orbitals [30]. The high electronegativity of Bi^{5+} and the $6s$ character of the orbitals lead to a low-lying CB [31] that does not involve the empty states of the other metal atoms. This is unlike the band anticrossing approach used in highly mismatched alloys, which relies on the interaction between localized dopant states and an extended semiconductor matrix to split the IB from the CB [32,33]. The presence of an IB in $\text{Ba}_2\text{ReBiO}_6$ materials suggests that it is possible to create IB states by substitution of Bi^{5+} into a transition-metal-based FE perovskite. For example, the substitution of as little as 5% Bi^{5+} into $\text{Ba}_2\text{InTaO}_6$ reduces E_g from 2.97 to 1.70 eV [34]. However, there are no reports of Bi^{5+} -doped ferroelectrics. We therefore use first-principles calculations to study the structural and electronic properties of $(1-x)\text{KNbO}_3-x\text{KBiO}_3$ (KNB), $(1-x)\text{Pb}_2\text{InNbO}_6-x\text{Ba}_2\text{InBiO}_6$ (PIN-BIB), and $(1-x)\text{Pb}_2\text{ScNbO}_6-x\text{Ba}_2\text{ScBiO}_6$ (PSN-BSB) solid solutions. We hypothesize that the combination of a ferroelectric end member and Bi^{5+} on the B site will reduce the band gap while preserving ferroelectricity.

II. METHODOLOGY

We performed density functional theory (DFT) calculations using the norm-conserving nonlocal pseudopotential plane-wave method [35]. The pseudopotentials [36] are

*rappe@sas.upenn.edu

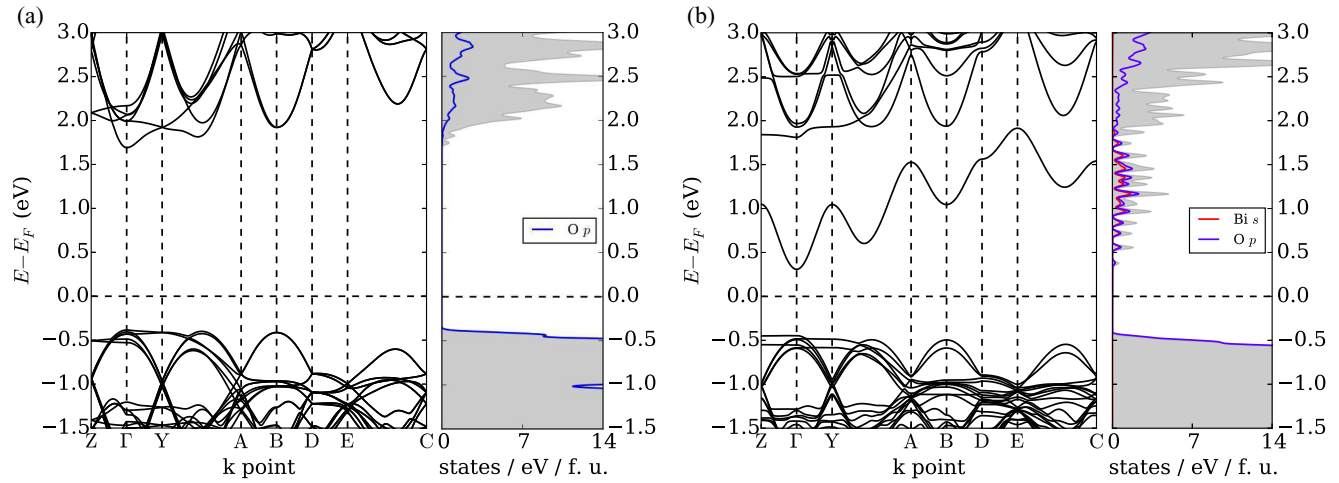


FIG. 1. (Color online) LDA + U band structures and PDOS of (a) KNO and (b) KNB; shaded areas indicate total DOS.

generated using the OPIUM package [37] with a 50 Ry cutoff of the kinetic energy. DFT calculations were done with the QUANTUM ESPRESSO package [38] using the local density approximation [39] and PBEsol [40] for the exchange-correlation functional for both structural optimization and electronic structure calculations. For a $2 \times 2 \times 2$ perovskite supercell, we used shifted $4 \times 4 \times 4$ and $8 \times 8 \times 8$ Monkhorst-Pack k -point grids [41] for the ground-state and the density-of-states (DOS) calculations, respectively. Polarization was calculated by the Berry phase approach [42,43] on an unshifted $4 \times 4 \times 20$ k -point grid, where the densely sampled direction is permuted in order to obtain all three polarization components. Due to the multivalued nature of polarization, we calculated the polarization change when the centrosymmetric nonpolar structure deforms to the relaxed low-symmetry structure. To explore the photovoltaic activity for the two Pb-based materials, we evaluate the short-circuit current under linearly polarized light [44] using shift-current calculations. We chose the $2 \times 2 \times 2$ supercell to allow for modeling different doping fractions of Bi^{5+} . For structural optimization, both internal coordinates and lattice vectors are relaxed. In order to correct for the band-gap underestimation in DFT due to the unphysical delocalization of the Kohn-Sham states [45] (especially prominent when the band edges are composed of strongly correlated d and f orbitals), we used the DFT + U method, in which the Hubbard U term accounts for the on-site repulsion of the correlated electrons [46].

For the KNB system, we performed calculations at $x = 0.125$, where one of the eight Nb atoms in the supercell is replaced by a Bi atom. For the Pb-based materials, the two B cations form a rock-salt ordering to reduce the long-range Coulombic interaction [47]. Electronic structures are calculated for $x = 0, 0.25, 0.5, 0.75$, and 1. The positions of the dopant Bi atoms are chosen so that the high-symmetry structure possesses inversion symmetry and has no spontaneous polarization.

III. RESULTS AND DISCUSSION

A. Bi^{5+} doping in KNbO_3

The calculated band structures and projected densities of states (PDOS) of KNbO_3 (KNO) and KNB with local-density

approximation (LDA) + U functionals are shown in Fig. 1. We added U terms to both the Nb $4d$ and the Bi $5d$ orbitals. The effective U values are determined by a linear response approach [48] to be 3.86 eV (Nb $4d$) for KNO, and 3.94 eV (Nb $4d$) and 1.11 eV (Bi $5d$) for KNB, respectively. The electronic properties of KNO and KNB are summarized in Table I. Note that the only significant effect of the Hubbard U term is to increase the E_g of KNO from 1.7 to 2.1 eV by raising the CB energy. The KNB band gap is insensitive to the addition of U because its IB has negligible Nb $4d$ or Bi $5d$ characters. The LDA + U band gap for KNO, although improved, is still 1 eV below the experimental value, in agreement with other theoretical predictions [49]. Use of PBEsol + U (which is designed for solids), LDA, and LDA + U all yield similar results for KNB. Therefore, we expect that the general trend of band-gap reduction by Bi^{5+} doping in KNbO_3 is accurately reproduced by LDA calculations.

Inspection of the KNB electronic structure [Fig. 1(b)] shows that when Bi^{5+} is substituted for Nb^{5+} , an IB emerges, while the CB and VB do not change significantly. From the PDOS, it is evident that the IB mainly comprises Bi $6s$ and O $2p$. Due to the presence of the IB, the LDA + U E_g drops from 2.1 eV for KNO to 0.8 eV for KNB. The 0.25 C/m^2 calculated polarization value of KNB shows that the solid solution is still FE after Bi^{5+} doping. Inspection of the KNB band structure shows strong dispersion of the IB, such that there is only a small band gap between the IB and the original CB. This is unfavorable for the potential use of KNB in multigap solar cells.

TABLE I. Electronic properties of KNO and KNB. Experimental band gap [50] and polarization [51] are available for KNO but not for KNB.

Method	E_g (eV)		P (C/m^2)	
	KNO	KNB	KNO	KNB
Experiment	3.1		0.41	
LDA	1.7	0.8	0.42	0.26
LDA + U	2.1	0.8	0.40	0.25
PBEsol + U	2.4	0.9	0.42	0.24

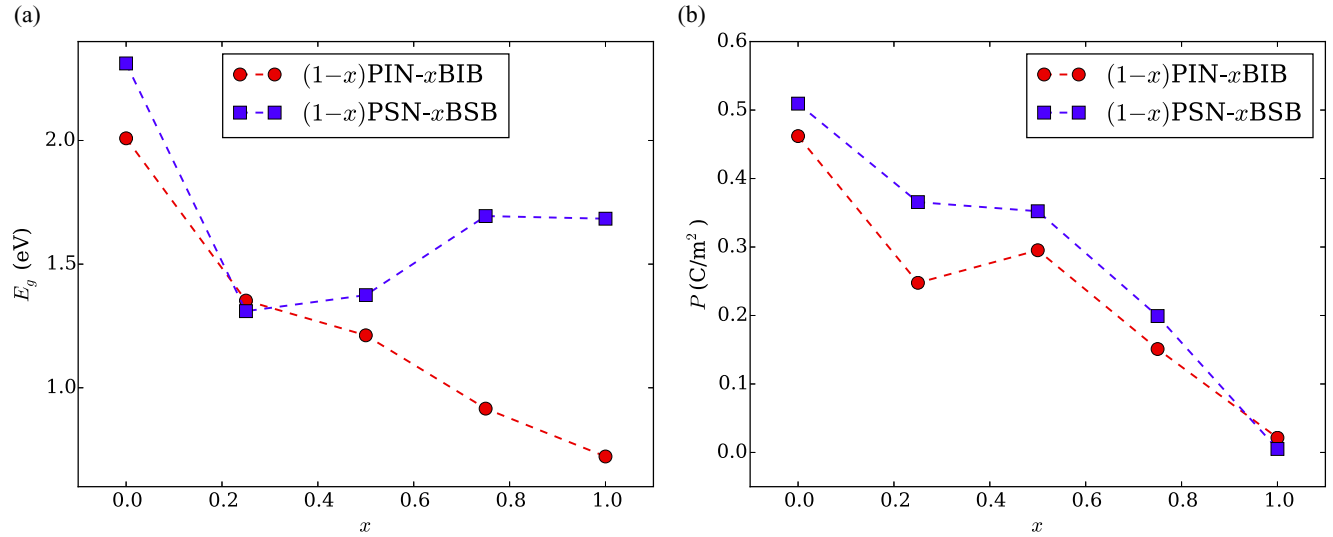


FIG. 2. (Color online) (a) LDA band gap and (b) polarization vs composition for PIN-BIB and PSN-BSB. x is the concentration of end member BIB or BSB.

Due to the large ionic radius mismatch between Nb^{5+} (0.64 Å) and Bi^{5+} (0.76 Å) on the B site and the fact that the end-member KBiO_3 does not form a stable perovskite phase [52], the KNB solid solution is unlikely to form with normal solid-state synthesis methods. It nevertheless serves as a proof of concept that lowering the band gap by “IB insertion” while maintaining strong P is possible for FE oxides.

B. Bi^{5+} doping in more feasible double perovskite systems

To suggest more feasible candidates for efficient solar-energy conversion, we examine solid solutions in which one end member is a naturally occurring perovskite with Bi^{5+} on the B site and the other is a FE perovskite. For better solubility, the lattice mismatch between end members should be kept to a minimum. Therefore, we studied the structural and electronic properties of PIN-BIB and PSN-BSB. The lattice parameters of these end members in the perovskite phase are PIN (4.11 Å) [53], BIB (4.23 Å) [54], PSN (4.08 Å) [55], and BSB (4.18 Å) [56], with both alloy pairs differing by less than 3%. We study the rock-salt ordered B -cation arrangement because it minimizes the Coulombic interaction between B cations with different charges. This B -cation ordering can be achieved in PSN and PIN with slow annealing, and both PSN and PIN exhibit ferroelectricity for ordered or partially ordered B -cation arrangements [57,58].

The calculated band gaps and polarizations for the two solid solutions at different doping concentrations are shown in Fig. 2. The polarization values generally decrease with increasing Bi^{5+} concentration, consistent with the decrease in the concentration of ferroelectrically active Pb and Nb ions. The effect of Bi^{5+} doping on the band gap is more complicated. For PIN-BIB, E_g decreases monotonically with increasing x , while for PSN-BSB, there is a minimum E_g at $x = 0.25$. At this concentration, Bi^{5+} causes a substantial decrease in E_g while still preserving a substantial polarization. In addition, the formation energies of PIN-BIB and PSN-BSB at $x = 0.25$ are both negative, indicating that these solid solutions are

energetically more favorable than their parent materials (See Fig. S1 in the Supplemental Material [59]). Therefore, we examine PIN-BIB and PSN-BSB at $x = 0.25$ more closely. The properties of PIN-BIB and PSN-BSB at $x = 0.25$ are summarized in Table II.

The band structures and PDOS with LDA functionals for the two solid solutions at $x = 0.25$ are shown in Fig. 3. From here on, we focus on studying solid solutions at $x = 0.25$, and the doping concentration will not be explicitly denoted. The reduction in band gap is caused by IBs that are of Bi $6s$ and O $2p$ origin. Comparison of KNB, PIN-BIB, and PSN-BSB band structures shows that Bi^{5+} introduces IBs, independent of the composition of the parent FE material. This suggests that Bi^{5+} substitution, if experimentally achievable, would lower the band gap of other FE perovskites as well. Figure 3 shows that PSN-BSB has an IB with a larger bandwidth than that of PIN-BIB. A more dispersive IB implies a lower effective mass for the electrons and more mobile carriers, which could allow for better conductivity for photoexcited electrons, whereas a narrower band (such as the one in PIN-BIB) indicates isolated Bi $6s$ states and lower probability of electron hopping between sites.

By comparing Fig. 3(a) to Fig. 3(b), it is evident that the difference in bandwidth is mostly the result of different dispersion behaviors of the IB at the E point (1/2, 1/2, 1/2), i.e., the IB energy at the E point is at minimum in PIN-BIB, but at maximum in PSN-BSB. At other high-symmetry points in the Brillouin zone, the dispersion trend is generally the same between the two solid solutions, with differences in the

TABLE II. Band gap E_g , polarization P , and lattice constants a , b , and c of 0.75PIN-0.25BIB and 0.75PSN-0.25BSB. Numbers in parentheses denote the three components of polarization.

	E_g (eV)	P (C/m ²)	a (Å)	b (Å)	c (Å)
PIN-BIB	1.4	0.25 (0.07, 0.21, 0.11)	8.26	8.25	8.34
PSN-BSB	1.3	0.37 (0.11, 0.33, 0.11)	8.16	8.16	8.16

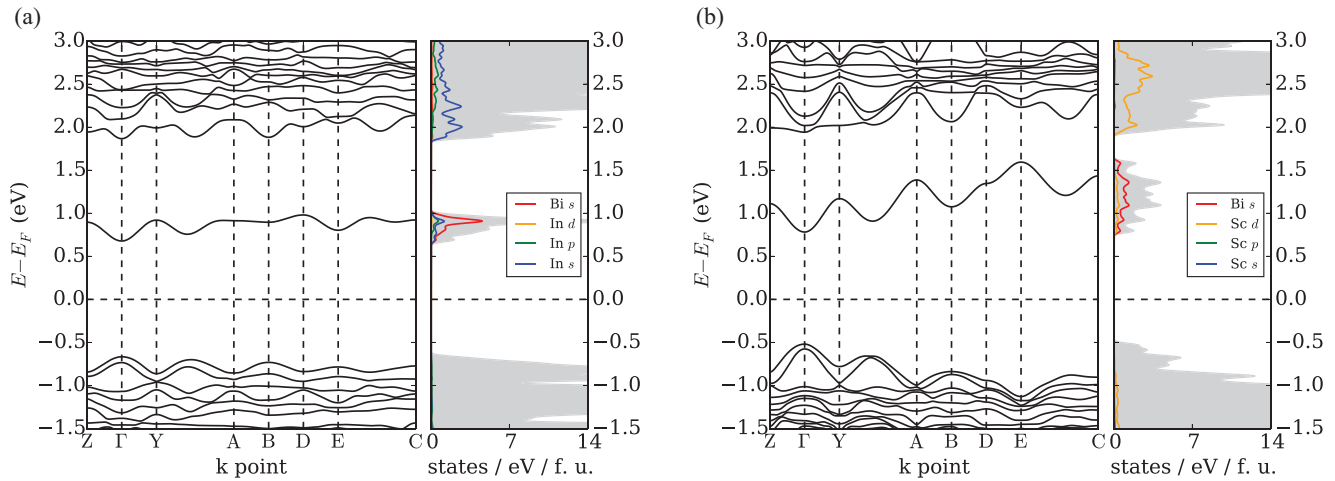


FIG. 3. (Color online) Band structures and PDOS for (a) PIN-BIB and (b) PSN-BSB; shaded areas indicate total DOS.

magnitude. We attribute the differing E -point dispersions to the atomic orbitals of In or Sc available to participate in IB formation. Consider a Bi-O- B' -O-Bi chain; at the E point, the wave-function periodicity requires that the two Bi atoms at the ends of the chain (in any direction) provide s orbitals of opposite phases to the IB, shown in Fig. 4. For B' , all orbitals that are symmetric with respect to the plane perpendicular to the O- B' -O line have an effectively nonbonding contribution to the IB because their constructive and destructive overlap with the two opposite phase O $2p$ lobes cancel each other. This leaves only p orbitals as possible participating orbitals to the IB. From the PDOS of PIN-BIB [Fig. 3(a)], we see that the valence $5p$ in In $^{3+}$ is readily available in the IB, which is reflected in the In p -O p σ bond shown in Fig. 4(a). On the other hand, for Sc $^{3+}$, $4p$ orbitals are too high in energy and $3p$ orbitals are too low, compared to the valence $3d$. The PDOS of PSN-BSB [Fig. 3(b)] shows negligible p contribution to the IB,

and the wave function in Fig. 4(b) contains a very small fraction of the Sc p -O p σ^* bond, possibly from antibonding interaction of the low-energy Sc $3p$ in the core state. The bonding vs antibonding characteristic explains the energy minimum in In-containing vs maximum in Sc-containing solid solutions.

For a more mathematical description of the IB dispersion difference between the Sc- and In-containing perovskites, we construct and fit a tight-binding model for perfect cubic PIN-BIB and PSN-BSB where O p , Bi s , B' s , B' p , and B' d are the basis orbitals, whose on-site energies are e_p , e_s , e'_s , e'_p , and e'_d , respectively. The hopping matrix elements that are considered in our model include t_{sp} ($\sigma_{\text{Bi}s \rightarrow \text{O}p}$), t'_{sp} ($\sigma_{\text{B}'s \rightarrow \text{O}p}$), t'_{pp} ($\sigma_{\text{B}'p \rightarrow \text{O}p}$), and t'_{dp} ($\sigma_{\text{B}'d \rightarrow \text{O}p}$). By minimizing the difference between the tight-binding band structure and the corresponding DFT band structure, we obtained the on-site energies and hopping terms listed in Table III. We show in Fig. 5 the comparison of the DFT and tight-binding band

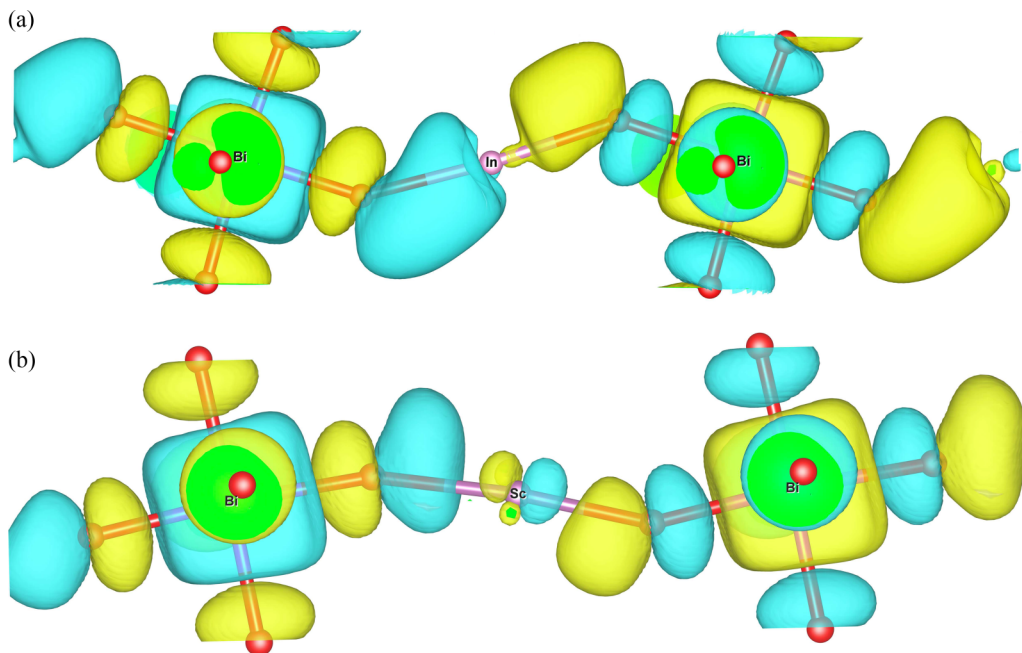


FIG. 4. (Color online) E -point intermediate-band wave functions along the Bi-O- B' -O-Bi chain in (a) PIN-BIB and (b) PSN-BSB.

TABLE III. Tight-binding model parameters of PIN-BIB and PSN-BSB fitted from corresponding DFT band structures.

e (eV)	PIN-BIB		PSN-BSB		t (eV)	PIN-BIB	PSN-BSB
Bi e_s	6s	1.25	6s	1.38	t_{sp} ($\sigma_{\text{Bi}s \rightarrow \text{O}p}$)	4.22	4.39
In/Sc e'_s	5s	2.69	4s	5.51	t'_{sp} ($\sigma_{B's \rightarrow \text{O}p}$)	1.39	0.41
In/Sc e'_p	5p	6.88	3p	-17.28	t'_{pp} ($\sigma_{B'p \rightarrow \text{O}p}$)	2.03	0.39
In/Sc e'_d	4d	-6.72	3d	4.16	t'_{dp} ($\sigma_{B'd \rightarrow \text{O}p}$)	0.55	2.91
O e_p	2p	0.00	2p	0.00			

structure for the two solid solutions, with the IB plotted as a band whose width at each k point represents the relative contribution from different B' atomic orbitals, in order to illustrate the difference in orbital contributions between PIN-BIB and PSN-BSB. Bi s and O p contributions are not shown because they are too large and overshadow the more delicate B' orbital contributions at different k points. It is clear that in PIN-BIB, the IB consists of mostly In s and some In p at the E point, whereas in PSN-BSB, the majority Sc orbital is Sc d . Note that in the DFT bands, we use a relaxed distorted

structure, which allows a little Sc d contribution at the E point, whereas in the tight-binding model, for simplicity a high-symmetry cubic structure is used, in which symmetry forbids any Sc d contribution at the E point.

From the fitting data, it is evident that in PIN-BIB, both s and p on-site energies are higher than the filled d orbitals, and the hopping from In s and In p to O p is more significant compared to the hopping from In d . For PSN-BSB, the p state is the filled core state with low on-site energy and interacts weakly with O p compared to the valence d states. The Sc s is valence, but still has smaller interaction with O p , leaving Sc d as the only orbital that has significant mixing with O. These results demonstrate that In s , In p , and Sc d are mostly favorable to participate in IB formation, with remarkable agreement between the DFT and tight-binding bands shown in Fig. 5.

C. Shift-current study of the Bi⁵⁺-doped double perovskites

Several mechanisms have been proposed to account for the photocurrent produced by FE materials under illumination. In thin films, excited carrier separation and the resulting

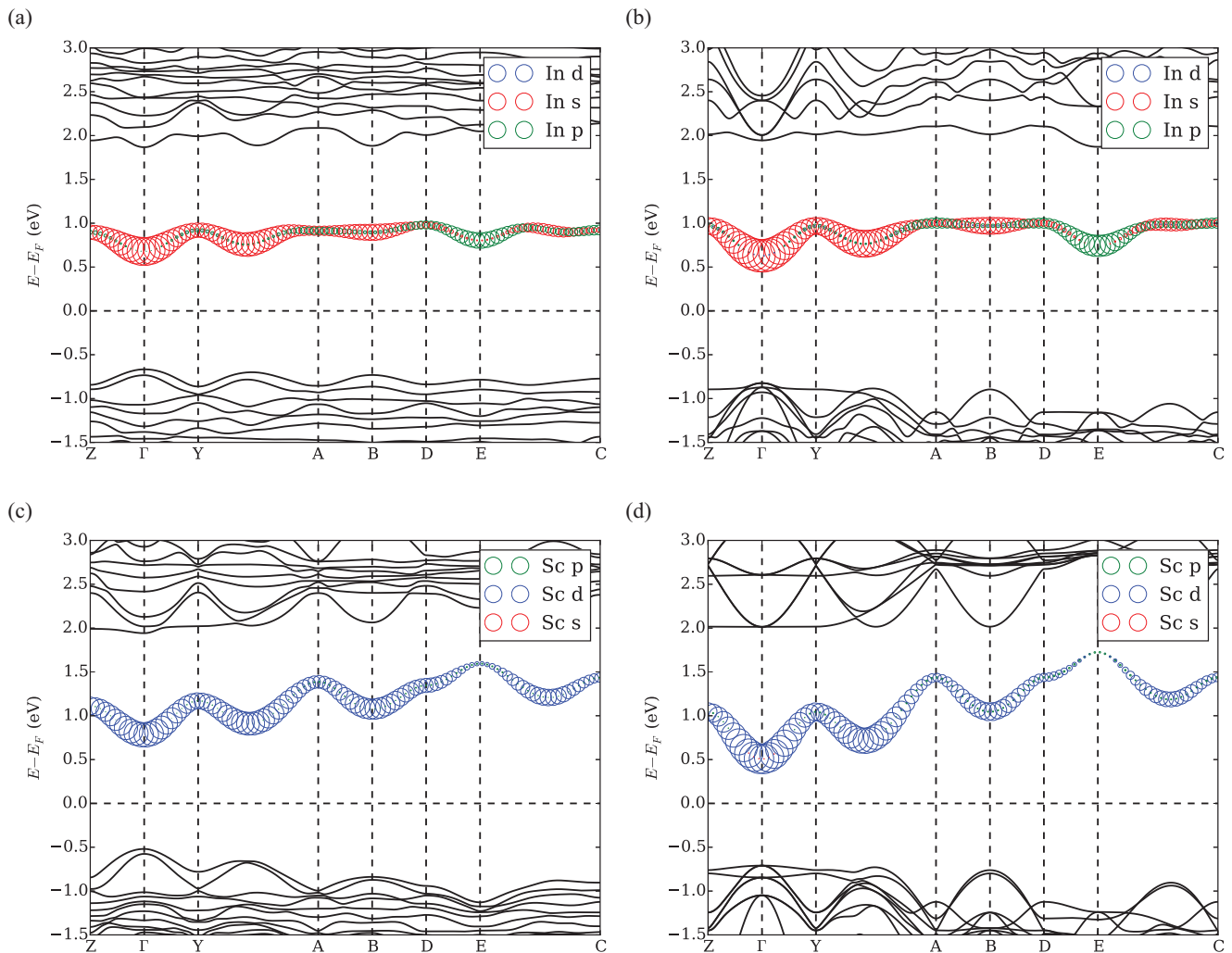


FIG. 5. (Color online) Comparison between (a),(c) DFT and (b),(d) tight-binding electronic bands for (a),(b) PIN-BIB and (c),(d) PSN-BSB. The intermediate bands are composed of circles whose centers reside on the corresponding energy levels and whose radii are proportional to the norm of the coefficients of the atomic orbital basis for the eigenstates at each k point.

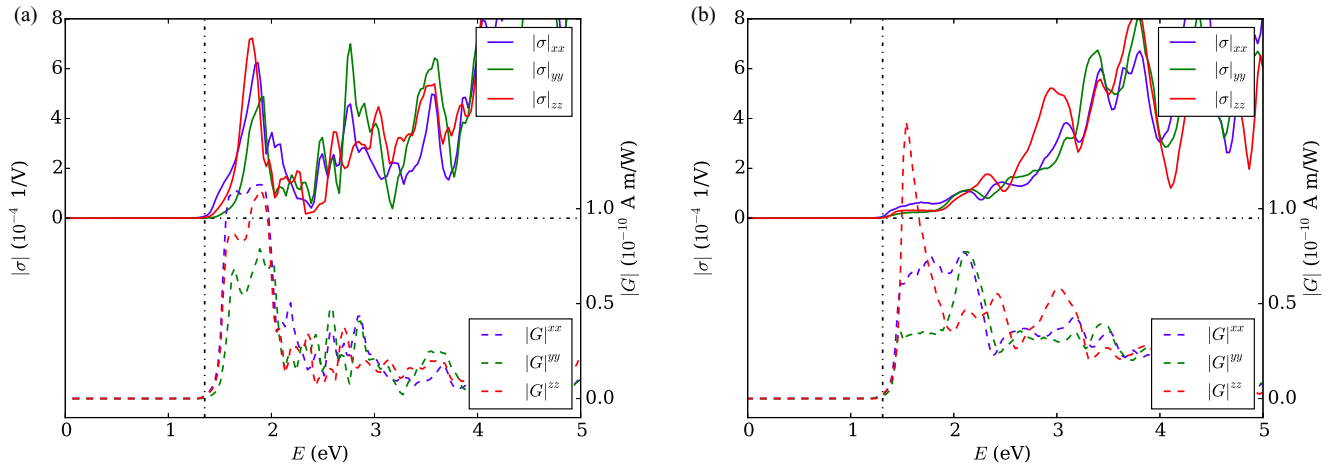


FIG. 6. (Color online) Total bulk photovoltaic susceptibility $|\sigma|$ (solid line) and Glass coefficient $|G|$ (dashed line) of (a) PIN-BIB and (b) PSN-BSB.

photovoltage and photocurrent have been ascribed to extrinsic effects such as engineered domain-wall structures and the depolarizing field due to incomplete polarization charge compensation at the ferroelectric-electrode interfaces [6,7]. In addition, an intrinsic bulk photovoltaic effect can also arise in a homogeneous noncentrosymmetric material, which is mainly governed by the shift-current mechanism [8–11]. Like the normal linear (in light intensity) interfacial photovoltaic effect, shift current is a second-order nonlinear optical effect with the photocurrent quadratic in the electric field (therefore linear in intensity). However, shift current does not rely on an externally engineered asymmetry or an internal depolarization field to separate charge. Under sustained illumination, electrons are continuously excited to a quasiparticle coherent state that is entangled with the radiation source, resulting in a net direct current due to the broken inversion symmetry. While we make clear that our designed materials can be useful as absorbers in conventional photovoltaics or by using the depolarization field at interfaces to separate charge (see Fig. S2 in the Supplemental Material [59] for the optical transition property), here we also study the bulk shift-current performance of these materials.

We calculated the shift-current susceptibility with respect to light intensity and the Glass coefficients of PIN-BIB and PSN-BSB. The shift current involves nonlinear optical processes that arise from the second-order interaction with incident electric field, in which electrons are excited to coherent superpositions, resulting in a net current flow in the presence of an asymmetric potential. The susceptibility σ_q^{rs} determines the current density J_q due to interaction with electric field E_r and E_s : $J_q = \sigma_q^{rs} E_r E_s$. For simplicity, we assume that both excitations are caused by the same monochromatic light, and thus only the diagonal terms σ_q^{rr} are reported. The Glass coefficient G_q^{rr} [4] is another measure of photovoltaic efficiency, the shift-current density for material of width w with incident light intensity I and frequency ω : $J_q(\omega) = G_q^{rr} I w$, assuming that the material is thick enough to absorb all incident light.

Figure 6 shows the calculated shift-current susceptibilities and the Glass coefficient spectra of PIN-BIB and PSN-BSB. It is immediately obvious that the photocurrent response thresholds of both materials are located at relatively low photon

energies—essentially at the theoretical band-gap edge. This verifies our expectation that the introduction of low-lying IB states would shift the light absorption and photocurrent response well into the visible-light range. Nevertheless, the two materials show quite different shift-current susceptibility behaviors. For PIN-BIB, one large peak appears in the near-band-gap region (at 1.9 eV) while no such peak is found in PSN-BSB. As the photon energy increases, the photocurrent response of PIN-BIB decreases and reaches a minimum at 2.3 eV. As illustrated by the band structure of PIN-BIB (Fig. 3), the large peak at 1.9 eV is mainly due to the transitions from the O $2p$ VB to the Bi $6s$ IB. Since this IB state is relatively localized and separated from the fundamental CB states, the photon absorption at higher energy is suppressed until the photon energy is large enough for a transition to the CB. For PSN-BSB, the shift-current susceptibility increases as a function of photon energy up to 4 eV. This broad-spectrum light absorption and photocurrent evolution is consistent with the dispersive IB in PSN-BSB. In addition, the magnitude of the shift-current susceptibility at the band edge is not as large as that in PIN-BIB. For both materials, the shift-current susceptibility exhibits similar behavior in terms of magnitude and spectrum shape under different polarizations of incident illumination.

The Glass coefficient gives the photocurrent density per unit sample width assuming full absorption, and includes the light-attenuation effect due to the absorption coefficient. As shown in Fig. 6, the Glass coefficient plots of both PIN-BIB and PSN-BSB exhibit a similar trend: a near-band-gap peak followed by decreasing intensity with higher incident photon energy, in contrast to the susceptibility plots in which PIN-BIB and PSN-BSB differ significantly. This is attributed to the relatively small absorption coefficients of PSN-BSB near the band gap with respect to PIN-BIB. The Glass coefficients in both materials show good photovoltaic activity within the visible range.

To evaluate the prospect of using these two materials for solar-energy conversion, we compare the calculated results to those of the prototype FE materials PbTiO_3 (PTO), BaTiO_3 (BTO), BiFeO_3 (BFO), and KNO . As shown in Table IV, the susceptibility magnitude of PIN-BIB near its band gap is larger than that of PTO and BTO. Although the shift-current response

TABLE IV. The calculated largest shift-current susceptibility σ and Glass coefficient G of various materials between the band gap E_g and 1 eV above it. For BFO, the numbers are calculated with the generalized gradient approximation (GGA) + U method [12] and those in parentheses are the experimental values, both with a photon energy of 2.85 eV [44,60].

	PIN-BIB	PSN-BSB	PTO	BTO	BFO	KNO
σ (10^{-4} V $^{-1}$)	7.2	1.7	3.9	1.4	0.9 (1.1)	11.1
G (10^{-10} A m/W)	1.1	1.4	1.2	0.2	0.05 (0.05)	0.3
E_g (eV)	1.4	1.3	3.4	3.2	2.7	3.1

of PSN-BSB near the band gap is not as large as that of PTO, the response at higher photon energy is stronger. The Glass coefficient magnitudes of both PIN-BIB and PSN-BSB in the near-band-gap region are also comparable to that of PTO and larger than that of BTO.

Clearly, the shift-current responses of PIN-BIB and PSN-BSB near their band gaps are much larger than the measured BFO value (near its higher E_g). Furthermore, the Glass coefficients of both PIN-BIB and PSN-BSB are at least one order of magnitude larger than the measured BFO value, implying their potential use as photovoltaic materials. Though the shift-current responses of PIN-BIB and PSN-BSB are not as large as that of KNO, the onset of photon absorption energy is again lower (1.4 vs 3.1 eV) and their Glass coefficients are more than twice that of KNO. Based on these comparisons and the fact that the shift-current response of PIN-BIB and PSN-BSB occurs at low photon energy, we propose that these two materials are promising candidates for bulk photovoltaic solar-energy conversion. Furthermore, PIN-BIB is more appropriate for monochromatic illumination with photon energy at the band gap, while PSN-BSB should offer good photovoltaic performance under broad-spectrum solar light illumination. Since the excitations from the IB to the CB are not included in the shift current, these materials

could be more appealing for photovoltaic applications than the shift-current results shown here after appropriate doping.

IV. CONCLUSIONS

In conclusion, we have shown that semiconducting ferroelectrics with band gaps in the visible range can be designed by Bi⁵⁺ substitution on the perovskite B site. The introduction of Bi 6s empty states in the band gap of the parent material leads to an E_g lowering of ≈ 1.5 eV, enabling the absorption of much more of the solar spectrum in FE-based devices. The resulting materials exhibit several interesting electronic structure features, most notably a dispersive intermediate band due to the Bi 6s states. We propose that PIN-BIB and PSN-BSB are promising candidates for bulk photovoltaic solar-energy conversion based on their band gaps, polarization, solubility, and photocurrent response, with PIN-BIB more appropriate for monochromatic illumination and PSN-BSB more suitable for solar light illumination.

ACKNOWLEDGMENTS

L.J. was supported by the US Air Force Office of Scientific Research under Grant No. FA9550-10-1-0248. I.G. was supported by the US Office of Naval Research under Grant No. N00014-12-1-1033. F.W. was supported by the US Department of Energy under Grant No. DE-FG02-07ER46431. S.M.Y. was supported by the National Science Foundation, under Grant No. DMR-1124696. P.K.D. and A.M.R. were supported by the Energy Commercialization Institute of BFTP. Computational support was provided by the High Performance Computing Modernization Office of the US Department of Defense, and the National Energy Research Scientific Computing Center of the US Department of Energy. We would like to thank Fan Zheng for fruitful discussions.

-
- [1] W. Shockley and H. Queisser, *J. Appl. Phys.* **32**, 510 (1961).
- [2] A. G. Chynoweth, *Phys. Rev.* **102**, 705 (1956).
- [3] F. S. Chen, *J. Appl. Phys.* **40**, 3389 (1969).
- [4] A. M. Glass, D. von der Linde, and T. J. Negran, *Appl. Phys. Lett.* **25**, 233 (1974).
- [5] V. M. Fridkin, *Crystallog. Rep.* **46**, 654 (2001).
- [6] M. Qin, K. Yao, and Y. C. Liang, *Appl. Phys. Lett.* **95**, 022912 (2009).
- [7] M. Qin, K. Yao, and Y. C. Liang, *Appl. Phys. Lett.* **93**, 122904 (2008).
- [8] G. Dalba, Y. Soldo, F. Rocca, V. M. Fridkin, and P. Saintavitt, *Phys. Rev. Lett.* **74**, 988 (1995).
- [9] R. von Baltz and W. Kraut, *Phys. Rev. B* **23**, 5590 (1981).
- [10] K. Tonooka, P. Poosanaas, and K. Uchino, *Proc. SPIE* **3324**, 224 (1998).
- [11] B. I. Sturman and V. M. Fridkin, in *Ferroelectricity and Related Phenomena*, edited by G. W. Taylor (Gordon and Breach, New York, 1992), Vol. 8.
- [12] S. M. Young, F. Zheng, and A. M. Rappe, *Phys. Rev. Lett.* **109**, 236601 (2012).
- [13] K. Nonaka, M. Akiyama, T. Hagio, and A. Takase, *J. Eur. Ceram. Soc.* **19**, 1143 (1999).
- [14] T. Choi, S. Lee, Y. Choi, V. Kiryukhin, and S.-W. Cheong, *Science* **324**, 63 (2009).
- [15] S. Y. Yang, J. Seidel, S. J. Byrnes, P. Shafer, C. H. Yang, M. D. Rossell, P. Yu, Y. H. Chu, J. F. Scott, J. W. Ager, L. W. Martin, and R. Ramesh, *Nat. Nanotechnol.* **5**, 143 (2010).
- [16] J. Seidel, D. Y. Fu, S. Y. Yang, E. Alarcon-Llado, J. Q. Wu, R. Ramesh, and J. W. Ager, *Phys. Rev. Lett.* **107**, 126805 (2011).
- [17] P. C. Joshi and S. B. Desu, *Thin Solid Films* **300**, 289 (1997).
- [18] D. Bao, X. Yao, K. Shinozaki, and N. Mizutani, *J. Physics D: App. Phys.* **36**, 2141 (2003).
- [19] S. Pandeya, A. Jamesa, R. Ramana, S. Chatterjee, A. Goyala, C. Prakasha, and T. Goelb, *Physica B* **369**, 135 (2005).
- [20] K. Y. Chan, W. S. Tsang, C. L. Mak, K. H. Wong, and P. M. Hui, *Phys. Rev B* **69**, 144111 (2004).

- [21] X. Wan, H. L. W. Chan, C. L. Choy, X. Zhao, and H. Luo, *J. Appl. Phys.* **96**, 1387 (2004).
- [22] J. W. Bennett, I. Grinberg, and A. M. Rappe, *J. Am. Chem. Soc.* **130**, 17409 (2008).
- [23] G. Y. Gou, J. W. Bennett, H. Takenaka, and A. M. Rappe, *Phys. Rev. B* **83**, 205115 (2011).
- [24] W. S. Choi, M. F. Chisholm, D. J. Singh, T. Choi, G. E. J., Jr., and H. N. Lee, *Nat. Commun.* **3**, 689 (2012).
- [25] I. Grinberg, D. V. West, M. Torres, G. Gou, D. M. Stein, L. Wu, G. Chen, E. M. Gallo, A. R. Akbashev, P. K. Davies, J. E. Spanier, and A. M. Rappe, *Nature (London)* **503**, 509 (2013).
- [26] A. Luque and A. Martí, *Phys. Rev. Lett.* **78**, 5014 (1997).
- [27] A. Martí, E. Antolín, C. R. Stanley, C. D. Farmer, N. López, P. Díaz, E. Cánovas, P. G. Linares, and A. Luque, *Phys. Rev. Lett.* **97**, 247701 (2006).
- [28] A. Luque, A. Martí, and C. Stanley, *Nat. Photon.* **6**, 146 (2012).
- [29] N. López, L. A. Reichertz, K. M. Yu, K. Campman, and W. Walukiewicz, *Phys. Rev. Lett.* **106**, 028701 (2011).
- [30] T. Hatakeyama, S. Takeda, F. Ishikawa, A. Ohmura, A. Kakayama, Y. Yamada, A. Matsushita, and J. Yea, *J. Ceram. Soc. J* **118**, 91 (2010).
- [31] S. G. Hur, T. W. Kim, S. J. Hwang, H. Park, W. Choi, S. J. Kim, and J. H. Choy, *J. Phys. Chem. B* **109**, 15001 (2005).
- [32] W. Shan, W. Walukiewicz, J. W. Ager, E. E. Haller, J. F. Geisz, D. J. Friedman, J. M. Olson, and S. R. Kurtz, *Phys. Rev. Lett.* **82**, 1221 (1999).
- [33] K. M. Yu, W. Walukiewicz, J. Wu, W. Shan, J. W. Beeman, M. A. Scarpulla, O. D. Dubon, and P. Becla, *Phys. Rev. Lett.* **91**, 246403 (2003).
- [34] T. W. Kim, S. G. Hur, S. J. Hwang, H. Park, Y. Park, W. Choi, and J. H. Choy, *Mater. Res. Bull.* **42**, 1914 (2007).
- [35] M. C. Payne, M. P. Teter, D. C. Allan, T. A. Arias, and J. D. Joannopoulos, *Rev. Mod. Phys.* **64**, 1045 (1992).
- [36] A. M. Rappe, K. M. Rabe, E. Kaxiras, and J. D. Joannopoulos, *Phys. Rev. B* **41**, 1227 (1990).
- [37] <http://opium.sourceforge.net>.
- [38] P. Giannozzi, S. Baroni, N. Bonini, M. Calandra, R. Car, C. Cavazzoni, D. Ceresoli, G. L. Chiarotti, M. Cococcioni, I. Dabo, A. D. Corso, S. de Gironcoli, S. Fabris, G. Fratesi, R. Gebauer, U. Gerstmann, C. Gougoussis, A. Kokalj, M. Lazzeri, L. Martin-Samos, N. Marzari, F. Mauri, R. Mazarello, S. Paolini, A. Pasquarello, L. Paulatto, C. Sbraccia, S. Scandolo, G. Sclauzero, A. P. Seitsonen, A. Smogunov, P. Umari, and R. M. Wentzcovitch, *J. Phys.: Condens. Matter* **21**, 395502 (2009).
- [39] J. P. Perdew and A. Zunger, *Phys. Rev. B* **23**, 5048 (1981).
- [40] J. P. Perdew, A. Ruzsinszky, G. I. Csonka, O. A. Vydrov, G. E. Scuseria, L. A. Constantin, X. Zhou, and K. Burke, *Phys. Rev. Lett.* **100**, 136406 (2008).
- [41] H. J. Monkhorst and J. D. Pack, *Phys. Rev. B* **13**, 5188 (1976).
- [42] R. D. King-Smith and D. Vanderbilt, *Phys. Rev. B* **47**, 1651 (1993).
- [43] R. Resta, *Ferroelectrics* **136**, 51 (1992).
- [44] S. M. Young and A. M. Rappe, *Phys. Rev. Lett.* **109**, 116601 (2012).
- [45] W. Kohn and L. J. Sham, *Phys. Rev.* **140**, A1133 (1965).
- [46] K. A. Johnson and N. W. Ashcroft, *Phys. Rev. B* **58**, 15548 (1998).
- [47] L. Bellaiche and D. Vanderbilt, *Phys. Rev. Lett.* **81**, 1318 (1998).
- [48] M. Cococcioni and S. de Gironcoli, *Phys. Rev. B* **71**, 035105 (2005).
- [49] C. Duan, W. N. Mei, J. Liu, and J. R. Hardy, *J. Phys.: Condens. Matter* **13**, 8189 (2001).
- [50] B. T. Matthias, *Phys. Rev.* **75**, 1771 (1949).
- [51] P. Günter, *J. Appl. Phys.* **48**, 3475 (1977).
- [52] T. N. Nguyen, D. M. Giaquinta, W. M. Davis, and H. zur Loye, *Chem. Mater.* **5**, 1273 (1993).
- [53] S. G. Zhukov, A. V. Yatsenko, and S. B. Vakhrushev, *J. Struct. Chem.* **38**, 486 (1997).
- [54] W. T. Fua, M. J. Polderman, and F. M. Mulder, *Mater. Res. Bull.* **35**, 1205 (2000).
- [55] K. S. Knight and K. Z. Baba-Kishi, *Ferroelectrics* **173**, 341 (1995).
- [56] M. W. Lufaso, P. W. Barnes, and P. M. Woodward, *Acta Crystallog. Sec. B* **62**, 397 (2006).
- [57] K. Ohwada and Y. Tomita, *J. Phys. Soc. Jpn* **79**, 011012 (2010).
- [58] J. Zhang, Q. Li, and D. Feng, *Chin. Phys. Lett.* **9**, 355 (1992).
- [59] See Supplemental Material at <http://link.aps.org/supplemental/10.1103/PhysRevB.90.075153> for formation energy, and imaginary part of the dielectric constants (as an indicator of optical transition property) of PIN-BIB and PSN-BSB.
- [60] W. Ji, K. Yao, and Y. C. Liang, *Phys. Rev. B* **84**, 094115 (2011).